Linna, Riku; Suhonen, P. M.; Piili, J.

Rigidity-induced scale invariance in polymer ejection from capsid

Rigidity-induced scale invariance in polymer ejection from capsid

R. P. Linna,[*] P. M. Suhonen, and J. Piili

Department of Computer Science, Aalto University, P.O. Box 15400, FI-00076 Aalto, Finland

(Received 20 July 2017; published 1 November 2017)

While the dynamics of a fully flexible polymer ejecting a capsid through a nanopore has been extensively studied, the ejection dynamics of semiflexible polymers has not been properly characterized. Here we report results from simulations of ejection dynamics of semiflexible polymers ejecting from spherical capsids. Ejections start from strongly confined polymer conformations of constant initial monomer density. We find that, unlike for fully flexible polymers, for semiflexible polymers the force measured at the pore does not show a direct relation to the instantaneous ejection velocity. The cumulative waiting time $t(s)$, that is, the time at which a monomer s exits the capsid the last time, shows a clear change when increasing the polymer rigidity κ. The major part of an ejecting polymer is driven out of the capsid by internal pressure. At the final stage the polymer escapes the capsid by diffusion. For the driven part there is a crossover from essentially exponential growth of t with s of the fully flexible polymers to a scale-invariant form. In addition, a clear dependence of t on polymer length N_0 was found. These findings combined give the dependence $t(s) \propto N_0^{0.55} s^{1.33}$ for the strongly rigid polymers. This crossover in dynamics where κ acts as a control parameter is reminiscent of a phase transition. This analogy is further enhanced by our finding a perfect data collapse of t for polymers of different N_0 and any constant κ.

I. INTRODUCTION

Due to advances in biosciences the behavior of macromolecules such as DNA and proteins has been under intensive study over the last two decades. Living cells rely heavily on these biopolymers, which are transported through membranes via various processes. The escape of DNA and RNA from viral capsids is one of the most important such transportation processes. Viruses work by injecting their DNA or RNA to the host cell. A multitude of viruses store their genome inside a more or less spherical shell and eject it to a host cell through a pore or a syringe. Some well-known examples are the T4 phage, the T7 phage, and the λ phage.

Neither biological nor theoretical perspectives of the mechanisms of packaging, activation, and release of DNA from viral capsids are thoroughly understood [1–3]. The motivation to understand fundamentals of this process is further enhanced by its potential applications in drug delivery and gene therapy [4]. Recently significant advancement was made in artificially storing data in DNA [5]. This could open up possibilities for storing human-generated data into capsids from where it could be retrieved by using sequencing techniques.

The field of biopolymer dynamics has inspired physicists, since it provides complex and theoretically challenging problems to study. Accordingly, also capsid ejection of polymers has been the subject of a number of theoretical treatments [6–10]. These theoretical treatments have been accompanied by a multitude of studies using computer simulations [11–18]. These studies have addressed the ejection of fully flexible polymers and as such provide important information on the fundamentals of ejection dynamics. The results obtained from them have relevance to viruses containing RNA, such as the polio virus [19], or single stranded DNA that eject their genome through a pore.

Semiflexible polymers have received considerably less attention in both theoretical and computational studies of capsid ejection [12,13,17,17,20–22]. The double stranded DNA (dsDNA) shows resistance to bending, which in some cases of polymer dynamics does not change the characteristics appreciably from those of the fully flexible chain [23]. However, taking into account the bending rigidity of the dsDNA is very important in cases where confined geometries are involved. In dsDNA ejection it is essential, since the size of viral capsids is typically of the same order as dsDNA's persistence length (∼50 nm [24]).

Here, we study the ejection of semiflexible polymer chains from a spherical capsid. Computer simulations are performed using our implementations of stochastic rotation dynamics and Langevin dynamics (LD). It has been observed that *in vivo* the temporal aspects of the process are governed by long pauses throughout the ejection [25]. Mahalik *et al.* were able to reproduce this in simulations of semiflexible polymers [17]. They also explained that the ejection speed is directly related to the angle of incidence to the pore. While the friction of the pore has an indisputable effect on translocation in real biological systems, in this paper, which is the third in the series of papers investigating capsid ejection for different relevant settings, we focus on the underlying general ejection process. In order to do this we have reduced the pore friction by implementing a pore that has a smooth geometry.

Using our general simulation model, we will study the ejection process for polymers of different bending rigidity. In our previous studies on capsid ejection of flexible polymers we showed that the ejection dynamics is governed by the force the polymer beads inside the capsid exert on the bead at the pore entrance [15,16]. As will be seen, this result cannot be generalized to semiflexible polymer chains.

The paper is organized as follows. In Sec. II we describe the used computational models and methods. Results are presented in Sec. III. Here, we first give an account of how the polymer packaging rate affects ejection in Sec. III A, after which we evaluate the contribution to dynamics coming

---

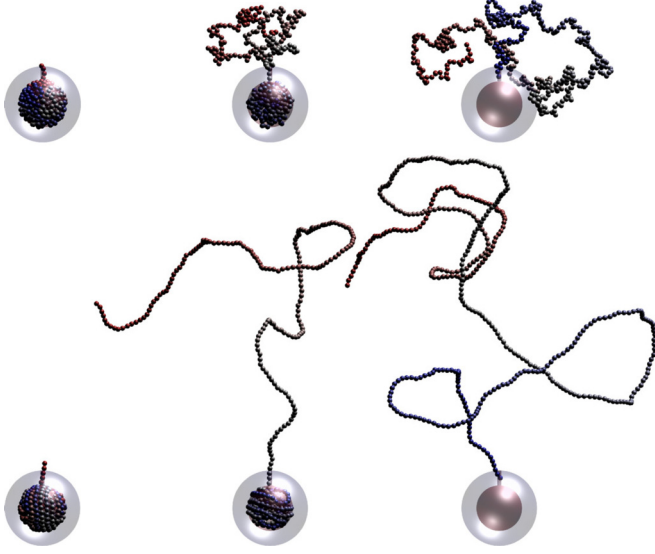[*]Corresponding author: riku.linna@aalto.fi

FIG. 1. Snapshots of capsid ejection simulations at the start of the simulation (left), halfway through translocation (middle), and in the end (right). Top row: Flexible chain ($\kappa = 0$). Bottom row: Semiflexible chain ($\kappa = 20$). Polymer length $N_0 = 400$ and initial monomer density $\rho_0 = 0.826$.

from the *trans* side, i.e., outside the capsid. Measurements of ejection times and pore force are reported and analyzed in Secs. III C and III D, respectively. The central results and analysis of the crossover of ejection dynamics with increasing polymer rigidity are given in Sec. III E. In Sec. III F we show that the measurement data describing ejection dynamics of polymers of the same rigidity but different length can be made to collapse onto a single curve. Results and conclusions are summarized in Sec. IV. The main result of the present paper is the observation that ejection dynamics enters a scale-invariant regime as polymer rigidity is increased.

II. MODELS AND METHODS

Here we present the computational model used in this paper. For the polymer we use a coarse grained beads-and-springs model with excluded volume interactions. The polymer is immersed in solvent modeled via stochastic rotation dynamics (SRD), which can be used to simulate hydrodynamical interactions. In addition to SRD, we use the computationally more effective Langevin dynamics to create initial conformations and measure pore force. The capsid is modeled as rigid walls with slip and no-slip boundary conditions for the polymer and the solvent, respectively. Since we focus on determining the generic ejection dynamics for semiflexible polymers in the same setting we have previously used for fully flexible polymers, we do not include electrostatic or hydration forces in our model. The simulation geometry and snapshots of an ejecting polymer are depicted in Fig. 1 for polymers of different persistence lengths.

A. The polymer model

The polymer is a chain of pointlike beads where each subsequent pair of beads is connected with the finitely extensible nonlinear elastic potential:

$$U_F = -\frac{K}{2}r_{max}^2 \ln\left[1 - \left(\frac{r}{r_{max}}\right)^2\right], \; r < r_{max}. \quad (1)$$

Here r is the distance between the two subsequent beads and K and r_{max} are potential parameters. Between all polymer beads we have the shifted and truncated Lennard-Jones (LJ) potential that accounts for the excluded volume interactions:

$$U_{LJ} = \begin{cases} 4.8\epsilon\left[\left(\frac{\sigma}{r_{ij}}\right)^{12} - \left(\frac{\sigma}{r_{ij}}\right)^6\right] + 1.2\epsilon, & r_{ij} \leqslant \sqrt[6]{2}\sigma \\ 0, & r_{ij} > \sqrt[6]{2}\sigma \end{cases}. \quad (2)$$

Here r_{ij} is the distance between beads with indices i and j. The potential is nonattractive everywhere and therefore models a good solvent. The parameters for the polymer potentials are chosen as $\sigma = 1.0$, $\epsilon = 1.0$, $K = 30/\sigma^2$, and $r_{max} = 1.5\sigma$ in reduced units.

To model bending rigidity we use the total bending potential of the form

$$U_{bend} = -\kappa \sum_i (\mathbf{r}_{i+1} - \mathbf{r}_i) \cdot (\mathbf{r}_i - \mathbf{r}_{i-1}), \quad (3)$$

where the parameter κ defines the strength of the bending potential so that persistence length grows with κ. In other words the potential resists bending and has its minimum when the polymer is straight.

B. The solvent and polymer dynamics

We use SRD to model the solvent in which the polymer is immersed (sometimes referred to as multiparticle collision dynamics) [26–28]. SRD models full hydrodynamic interactions as well as thermal fluctuations. It is also computationally effective and allows for switching off hydrodynamic interactions when needed.

The SRD solvent consists of pointlike particles that are propagated in two alternating steps: the *collision step* and the *streaming step*. In the streaming step the particles' positions are updated using the update rule

$$\mathbf{r}_i(t + \Delta t) = \mathbf{r}_i(t) + \mathbf{v}_i(t)\Delta t, \quad (4)$$

where $\mathbf{r}_i$ and $\mathbf{v}_i$ are the position and velocity of the particle i, respectively. Δt is the SRD time step. For the collision step, the particles are divided into a grid of cubic cells of edge length 1. In each cell the velocities of the particles are updated via the formula

$$\mathbf{v}_i(t + \Delta t) = \mathbf{v}_{cm}(t) + \Omega[\mathbf{v}_i(t) - \mathbf{v}_{cm}(t)], \quad (5)$$

where $\mathbf{v}_{cm}$ is the center of mass of the cell and Ω is a rotation matrix unique for the cell. The rotation matrix Ω has a rotation angle $3\pi/4$ and its rotation axis is randomly chosen for each cell each time step. The rotation angle defines the viscosity of the solvent. The collision step conserves energy and momentum in each cell. To preserve Galilean invariance the collision grid is shifted randomly at each step [29]. Between collision steps the random parts of the velocities of the solvent particles are scaled such that the solvent stays at the constant temperature of $kT = 1.0$ [30].

The polymer is integrated in time using the velocity Verlet algorithm with time step $\delta t = 0.0002$ [30,31]. Such a small time step was chosen to avoid cumulation of numerical errors due to the high monomer densities inside the capsid. For SRD we use the time step of $\Delta t = 0.5$. The polymer is coupled to the SRD solvent via the collision step where the polymer particles and solvent particles are treated similarly. Velocity Verlet and SRD algorithms take turns such that after $\Delta t / \delta t = 2500$ velocity Verlet steps a single SRD step is taken. The solvent particles have mass $m_s = 4$ and the polymer particles have mass $m_b = 16$.

One of the benefits of SRD is that we can switch hydrodynamics off in order to better understand its effects. This is achieved by randomly interchanging the velocities of each particle every step so that the hydrodynamic correlations vanish.

In addition to SRD, we use Langevin dynamics to model solvent in force measurements and polymer packaging due to its superior computational efficiency. In [16] we showed that LD and SRD without hydrodynamics yield similar results. LD follows the Langevin equation

$$m_b \frac{d\mathbf{v}_i}{dt}(t) = -\xi m_b \mathbf{v}_i(t) + \boldsymbol{\eta}_i(t) + \mathbf{f}_i(t), \qquad (6)$$

where ξ is the friction constant, $\boldsymbol{\eta}_i(t)$ is a random force exerted on the bead i, and $\mathbf{f}_i(t)$ includes all the external forces exerted on the bead i. We integrate the Langevin equation in time using Ermak's implementation [32]. The LD parameters were matched to those of SRD according to [16]. The time step in LD simulations was chosen to be $\delta t = 0.001$. In LD hydrodynamics is not included, but the solvent constitutes a Brownian heat bath.

C. The simulation geometry

The simulation geometry is depicted in Fig. 1. The polymer ejects from the inside (i.e., the *cis* side) to the outside (i.e., the *trans* side) of the spherical capsid shell through a narrow pore. In the initial state before ejection there are N_0 beads inside the capsid and a tail of four beads in the pore and outside the capsid. Therefore, the total length of the polymer is $N_0 + 4$. The thickness of the capsid shell is 3. The radius R_0 of the inner shell of the capsid depends on the chosen initial monomer density ρ_0 and N_0 via

$$\rho_0 = \frac{N_0}{\frac{4}{3}\pi (R_0 + \zeta)^3}, \qquad (7)$$

where $\zeta = 0.3$ is added to the capsid radius to account for the portion of the beads' volume residing outside the capsid inner wall. After this correction the measured pore forces collapse when plotted as a function of density for fully flexible polymers [16] (there defined as effective density). In other words, for fully flexible polymers of different lengths the force measured at the pore is approximately the same when the monomer density inside the capsid $\rho = 3N/[4\pi(R_0 + \zeta)^3]$ is the same. N is the number of monomers inside the capsid. In some publications volume fraction $\phi_0 = 4/3\pi(0.5)^3 \rho_0 \approx 0.52 \rho_0$ is used instead (the LJ potential implies monomer radius of ~ 0.5). In addition, in many studies a hard-sphere potential is used. Accordingly, the values for densities in studies by
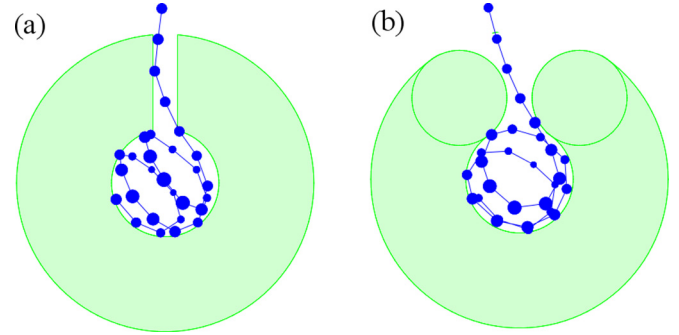

FIG. 2. Two-dimensional projection of the capsid geometry with different pores. The initial configuration of a polymer of length $N_0 = 25$ in capsids of initial monomer density $\rho_0 = 0.75$ is shown with (a) cylinder pore and (b) torus pore (monomer radius depicts distance from the viewer).

different authors are not directly comparable. The typical and the maximum monomer densities used here are $\rho_0 = 0.75$ and 0.826, which correspond to $\phi_0 = 0.39$ and 0.43. These volume fractions are within the correct range for real viral DNA. In what follows, the initial monomer density $\rho_0 = 0.75$, unless otherwise noted.

To model the pore, we use a torus shaped opening in the capsid shell as depicted in Fig. 2(b). We also compare this pore model to the more conservative cylinder pore [see Fig. 2(a)]. It is evident that the form of the pore has an effect on ejection dynamics. This is especially true for polymers exhibiting high bending resistance, since they must straighten considerably in the pore region to eject. This effect has been previously seen in Ref. [17] where the approach angle to the pore during ejection was observed to determine the momentary ejection rate. We use the smoother toroidal pore to attenuate these effects so as to make more general inferences of the escape process.

The whole capsid geometry is created using constructive solid geometry technique [33], which we have implemented for use in our simulations. In the simulations using a cylinder pore, the inner sphere and the pore (cylinder) are subtracted from the outer sphere [capsid = sphere$_{\text{out}}$ − sphere$_{\text{in}}$ − cylinder$_{\text{pore}}$]. In the torus pore model the geometry is a bit more complicated. The inner part of the torus is obtained by an intersection with a cone, after which a union is taken of this intersection and the sphere shell cut by a similar cone [capsid = (sphere$_{\text{out}}$ − sphere$_{\text{in}}$ − cone) ∪ (torus ∩ cone)]. See Fig. 2 for illustrations of the resulting geometries. The method tracks intersections with the particles' trajectories and capsid walls. The interaction between the capsid and the polymer is implemented using slip boundary conditions. For the solvent we use no-slip boundary conditions, which make the solvent velocity at the boundary disappear [34]. The pore radius is 0.4 for the polymer and 0.8 for the solvent. The larger pore for the solvent allows for smoother fluid flow in the pore region.

D. Creating initial polymer conformations

Experiments indicate that DNA is heavily organized inside capsids [35]. This raises the question of how the polymers should be packaged for ejection simulations. For semiflexible polymer chains the method of packaging has been observed

to have a tremendous impact on the resulting conformations [36–38]. Also in Ref. [17] it was observed that the magnitude of the packaging force affects the ejection rate of the polymers. Knots induced by packaging are also known to slow down the ejection [20,39].

As in the present paper the focus is on ejection dynamics for polymers of different lengths, we paid special attention in creating initial conformations in a consistent way such that the ejections with different parameters can be compared. We package the polymer inside the capsid one bead at a time and let the polymer relax in between the packaging steps. A resemblant packaging scheme is used in Ref. [40] where it is justified by the way adenosine triphosphate (ATP) driven packaging might occur in viral capsids.

Before starting the packaging, we place the last bead to eject in the middle of the pore and generate the rest of the polymer on the trans side as a self-avoiding random walk. After this, we drag beads one at a time from outside into the pore with a harmonic force $\mathbf{f}_{i,\mathrm{drag}} = 100 \cdot (\mathbf{r}_{\mathrm{midpore}} - \mathbf{r}_i)$. When a bead arrives to the middle of the pore, we pause the packaging for a time t_{eq} by fixing the dragged bead in place with different harmonic force $\mathbf{f}_{i,\mathrm{fix}} = 1000 \cdot (\mathbf{r}_{\mathrm{midpore}} - \mathbf{r}_i)$. This allows the polymer segment inside the capsid to relax. After the time t_{eq} has passed, the bead is guided into the capsid with a force of magnitude 100 and the next bead is dragged into the pore. With a long enough time t_{eq} between injecting new beads, we are able to generate initial configurations that are close to equilibrium. During packaging the polymer dynamics is propagated in time using LD instead of SRD. This is done due to SRD simulations being computationally intensive for large intermediate equilibration times t_{eq}. Using LD is justified here, since hydrodynamics has no effect on this slow packaging dynamics.

As we will show in Sec. III A, the ejection times depend on the equilibration time t_{eq} used during the packing process. Therefore, to create packed configurations for ejection simulations, we choose a t_{eq} large enough so that the ejection times seem to have converged. This way we ensure that polymers of different lengths are packaged in a consistent way.

E. Pore force

For fully flexible polymers waiting times $t_w(s)$ (i.e., the time it takes for bead s to eject the capsid the last time after bead $s - 1$ has ejected the capsid the last time) reflect the force $f(s)$ measured at the pore [15,16]. To see if this is the case also for semiflexible polymers we measure $f(s)$. The measurement is performed in the same way as polymer packaging, only in the opposite direction. We start the measurements from the same initial conformations as the ejection simulations. Instead of fully releasing the polymer, we first hold the bead $s = 1$ at the pore center by a harmonic force for a time $t_{\mathrm{eq}} = 2000$. After this we measure the force average for $t_{\mathrm{mt}} = 2000$ time units while still holding the polymer in place. Next, the bead $s = 2$ is pulled to the pore using a harmonic force and a similar equilibration and averaging is performed as for the first bead. We repeat this process for all beads and finally obtain the measured force for each s.

The measured $f(s)$ is the absolute value of the force having the sign of the z component of the force (the z axis points

TABLE I. Average bond length b and persistence length λ_p for different values of bending potential parameter κ, measured for polymer of length $N_0 = 25$ in free solvent.

κ	b	λ_p
0	0.980	0.889
5	0.988	4.35
10	1.00	9.41
15	1.01	15.3
20	1.03	21.9

outward and passes through the middle of the pore):

$$f(s) = \frac{1}{J} \sum_{j=1}^{J} \mathrm{sgn}[\mathbf{f}_{j,z}(s)]|\mathbf{f}_j(s)|, \qquad (8)$$

where j is the index of an individual simulation, and $\mathbf{f}_j(s)$ is the time average of the force over the measurement time t_{mt} in simulation j. J is the number of simulations. The sign function is used to cope with occasionally inward-pointing force at large s, where force due to pressure inside the capsid has decayed to a low magnitude. The absolute value describes the ejection force better than just the z component, because polymers of higher bending rigidity usually eject in a direction, which is at an angle to the pore axis z.

F. About persistence length and unit mapping

Previously, we have studied the ejection of fully flexible polymers [14–16]. The main interest has been in understanding general aspects of the process by minimizing the details involved. While fully flexible polymers are suited for describing single stranded DNA and RNA, a vast number of biologically relevant capsid ejections involve double stranded DNA. In such systems, bending rigidity cannot be omitted. Here we compare the polymer model used here to the real DNA using a simple unit mapping.

For polymers in our model, the Lennard-Jones potential implies the width of ~ 1 simulation units. Hence, a single simulation length unit can be taken to correspond to the width of dsDNA, which is about 2 nm. The persistence length λ_p can be adjusted via the bending parameter κ. By simulating a polymer in free solvent and measuring the angle θ between adjacent bonds and bond length b, we can compute the persistence length using the relation [41]

$$\lambda_p = \frac{b}{-\ln\langle \cos\theta \rangle}. \qquad (9)$$

The values of λ_p (in simulation units) for a few different values of κ are presented in Table I. The persistence length of real dsDNA is about 50 nm, and therefore we can conclude that $\kappa = 20$ best describes the properties of the dsDNA in our simulations. However, to obtain the best possible understanding of the effects of bending rigidity, we perform simulations with multiple values of κ.
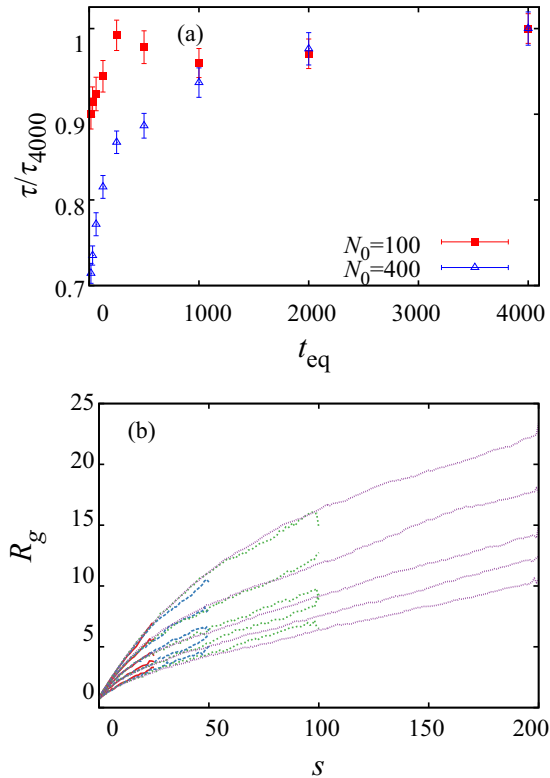
FIG. 3. (a) Ejection times when different equilibration times are used $\tau(t_{eq})$ normalized by $\tau(t_{eq} = 4000) \equiv \tau_{4000}$. LD and the cylinder pore model are shown. The initial densities are $\rho_0 = 0.743$ and 0.826 for $N_0 = 100$ and 400, respectively, and $\kappa = 20$. Error bars depict the standard deviations of the mean. (b) Radius of gyration R_g on the trans side during ejection for polymers of different length N_0. From top down $\kappa = 20, 10, 5, 2.5$, and 0.

III. RESULTS

Here, we present the results obtained from our SRD and LD simulations. All the presented quantities are arithmetic means over at least 45 independent simulations. In some cases more simulations were run in order to obtain better statistics.

A. Packaging rate

As discussed in Sec. II D, it is expected that when the polymer has bending rigidity, packaging affects the obtained initial polymer conformations and ejection times [17]. In order to define a consistent packaging method, we measured the ejection time τ as a function of the time t_{eq} used to equilibrate the polymer for each s during the packaging (see Sec. II D). This is shown in Fig. 3(a) for polymers of lengths $N_0 = 100$ and 200 and for $\kappa = 20$, simulated using LD and the cylinder pore.

We found that the longer the polymer is allowed to equilibrate during packaging the slower becomes the ejection. This is in agreement with the observation that polymers that were packaged using a higher force eject faster [17]. The faster ejection of more rapidly packaged polymers occurs due to the polymer not having sufficient time to relax to an equilibrium conformation. After the polymer is packaged its conformational changes are extremely slow due to high energy

barriers and therefore it remains in its local energy minimum. The local energy minima are deeper for a conformation that is closer to equilibrium, which slows down ejection.

Evidently, during packaging longer t_{eq} is required for longer polymers, as seen in Fig. 3(a). Using $t_{eq} = 2000$ is seen to result in sufficiently equilibrated conformations at least for $N_0 \leqslant 200$. In addition, the effect of t_{eq} on ejection times was seen to diminish for $\kappa = 0$ (not shown). Consequently, $t_{eq} = 2000$ is a judicious choice for our simulations.

B. Friction on the trans side

To guide the analysis of the ejection dynamics we first evaluate the contribution from the trans side friction, which has been shown to slow down ejection of semiflexible polymers [13]. Figure 3(b) shows the measured radius of gyration R_g of the ejected polymer segment. On each point on the s axis there is an identical number of beads on the trans side. As expected, R_g increases with κ. It is seen that R_g grows fairly similarly with s for different N_0, particularly for rigid polymers. Therefore, it is reasonable to expect that for all s the trans side friction is very similar for semiflexible polymers of different length. On the other hand, for polymers of low rigidity the trans side friction is small, as was shown for $\kappa = 0$ [16]. Accordingly, the trans side friction does not cause differences between polymers of different length and the obtained characteristics are explainable by friction and conformational changes on the cis side.

C. Characterization of dynamics via ejection time

We mainly use our implementation of the low-friction torus pore in order to more sensitively capture the dynamical characteristics of ejection. To validate the pore model and further our understanding of the ejection dynamics we make some comparison to the higher-friction cylinder pore used in our previous work.

Figure 4(a) shows the ejection time τ as a function of polymer length N_0 for various values of κ for the torus pore with included hydrodynamics. τ is seen to increase monotonically with κ for all N_0. Hence, for polymers of increased rigidity the effects of increased friction and less malleable conformations dominate over the increased force due to confinement driving the polymer out of the capsid.

For all κ, ejection times follow closely the scaling relation $\tau \sim N_0^\beta$. Scaling of τ with N_0 for the cylinder pore is equally good (not shown). τ as a function of rigidity κ are shown in Fig. 4(b). The obtained β are given in Table II. Due to volume correction, Eq. (7), β for $\kappa = 0$ are slightly greater than those reported in [16]. The two pores give consistent results. For the cylinder pore the β exponents are smaller due to the larger pore friction, increasing of which takes β closer to 1. β is seen to increase with κ for $\kappa \leqslant 10$. This trend breaks down for $\kappa = 20$, indicating a change in the dynamics.

Hydrodynamics is seen to speed up equally the ejection of polymers for all κ. Both the hydrodynamic interactions and larger κ increase the polymer's correlation length but have opposite effect on ejection rate. The correlation length increases by hydrodynamics due to momentum mediated by the solvent, which assists polymer motion. In contrast, the
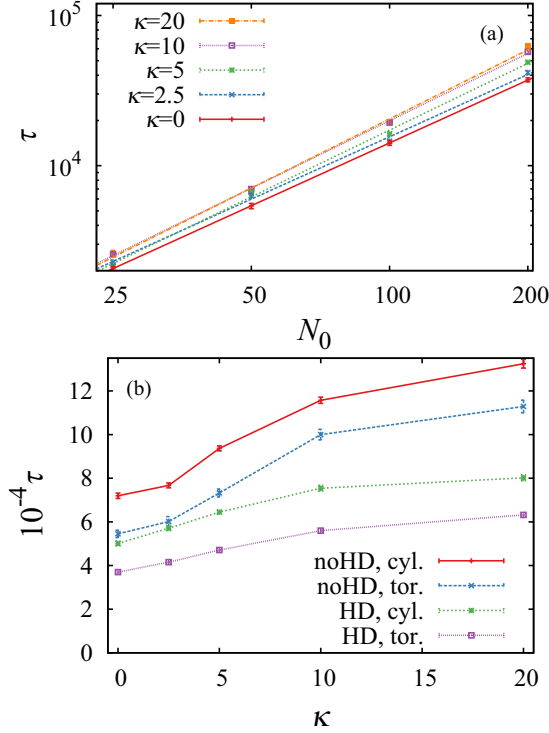
FIG. 4. (a) Torus pore, with hydrodynamics enabled. Ejection time τ is shown vs polymer length N_0 for different κ and for $N_0 = 25$, 50, 100, and 200. Lines show the relation $\tau \sim N_0^\beta$ fitted to the data. Logarithmic scale is used. The standard deviations of the mean are of the same order as the size of the points. (Values of β are shown in Table II.) (b) Ejection time τ as a function of κ for the cylinder and torus pores with and without hydrodynamics for $N_0 = 200$.

increased correlation length due to bending rigidity does not involve momentum transfer but only increases friction exerted on the moving polymer segment. In the presence of hydrodynamics, where correlation length is already increased, increasing κ does not increase correlation length further as in the absence of hydrodynamics. Consequently, the ejection time does not increase with κ as much when hydrodynamics is included, as seen in Fig. 4(b). Hydrodynamics is also seen to reduce β, the only exception being the case $\kappa = 20$, which was found to differentiate from ejections for smaller κ also in how β changes with κ. The reason for this difference

TABLE II. The fitted exponents in the relation $\tau \sim N_0^\beta$ for different values of bending parameter κ with and without hydrodynamics (HD), for the torus and the cylinder pore.

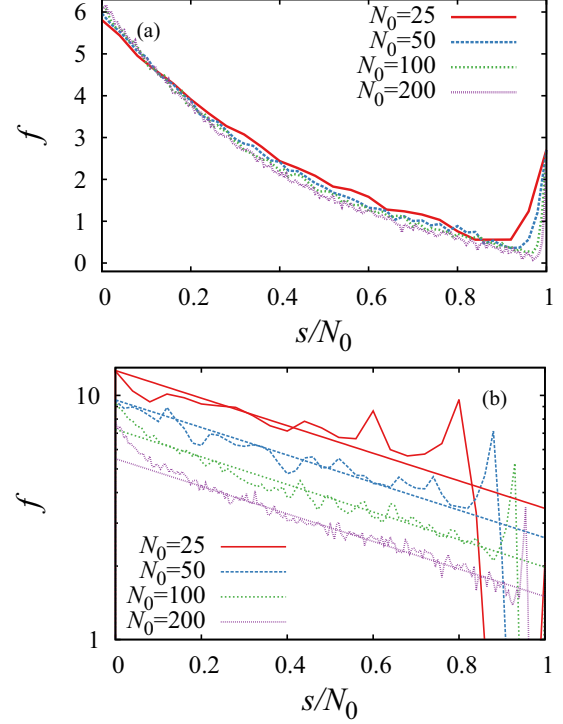|	Torus		Cylinder	
κ	No HD	HD	No HD	HD
0	1.43	1.39	1.46	1.35
2.5	1.48	1.38	1.41	1.37
5	1.53	1.48	1.43	1.39
10	1.57	1.49	1.45	1.40
20	1.48	1.53	1.35	1.39

FIG. 5. Equilibrium force f measured at the pore as a function of normalized number of ejected monomers s/N_0 for (a) $\kappa = 0$ and (b) $\kappa = 20$. The lines show $f = 12.4883(1/N_0)^{0.4} \exp(-1.3s/N_0)$.

can be understood by studying the cumulative waiting times (see Sec. III E).

D. Pore force

Figure 5(a) shows the equilibrium force f measured at the pore for fully flexible ($\kappa = 0$) polymers as a function of the number of ejected monomers normalized by the polymer length s/N_0. f for different N_0 essentially collapse when plotted this way. This means that the pore force is essentially a function of density inside the capsid. In addition, f is closely reminiscent of the inverse of the resulting waiting time profile $1/t_w$ where $t_w(s)$ is the elapsed time between the last ejections of monomers s and $s + 1$ [15,16]. Consequently, the cumulative waiting time $t(s) = \int_0^s t_w(s')ds'$ in Fig. 7 is closely related to $f(s)$ for $\kappa = 0$.

As κ increases f is no longer constant for constant s/N_0. With $\kappa = 20$, f for different N_0 has roughly the dependence $f \propto (1/N_0)^{0.4} \exp(-1.3s/N_0)$ [see Fig. 5(b)]. Due to starting all ejections from a constant monomer density, N_0 is proportional to V, where V is the capsid volume [see Eq. (7)]. Hence, $f \propto (1/V)^{0.4}$. For the constant $\kappa = 20$ the persistence length is constant for all N_0. The force exerted on the capsid wall increases with λ_p/R_0. Writing $f \propto (\lambda_p/R_0)^\gamma$ and using $f \propto 1/V^{0.4}$ gives $\gamma \approx 1.2$. A value $\gamma \gtrsim 1$ is plausible. For one semiflexible beam crossing through the midpoint of the capsid and touching opposite walls one would expect γ of the order of 1. In the actual polymer conformation with intertwined semiflexible lobes pressing against each other and the walls the increase of f with λ_p is expected to be superlinear. The dependence $f \propto (1/N_0)^{0.4}$ implies the breakdown of the
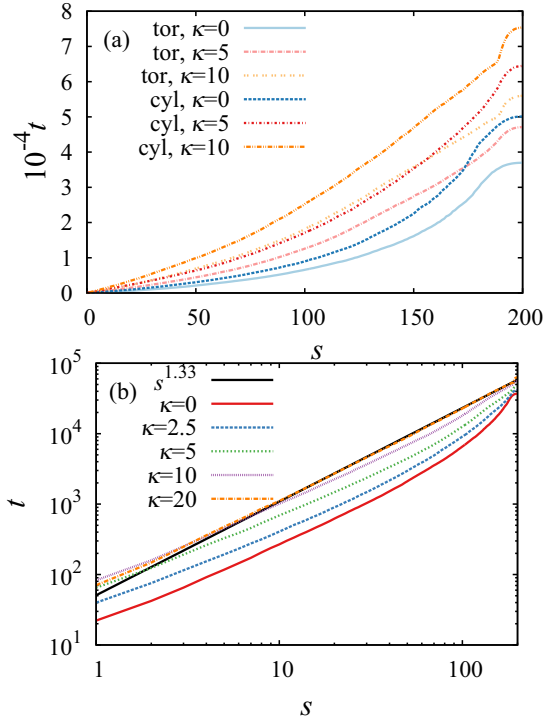
FIG. 6. (a) Cumulative waiting times $t(s)$ for the torus (tor.) and cylinder (cyl.) pore models using $\kappa = 0, 5$, and 10. $N_0 = 200$, $\rho_0 = 0.75$. (b) Torus pore. Cumulative waiting times are shown for polymers of length $N_0 = 200$ and for different κ. The black solid line shows the scaling $t \sim s^{1.33}$.

above-described direct relation of f and $1/t_w$ for more rigid polymers. In other words, as κ increases ejection dynamics is less directly related to the force measured at the pore, as already evidenced by the rigid polymers ejecting slower than more flexible polymers in spite of the spring force increasing with rigidity (see Fig. 4).

In Fig. 5(b) f is seen to decay to zero at $s/N_0 < 1$ for all N_0, which occurs when the polymer segment inside the capsid touches the capsid only at the pore. Just before this decay, there is a peak in each f vs s/N_0 curve. This takes place when the semirigid ($\kappa = 20$) polymer segment inside the capsid barely extends from the pore to the capsid inner wall. At this point most of the force induced by the bending rigidity is directed toward the positive z direction (exit direction) in the pore. Consequently, the z-directional force measured at the pore is largest when the length of the polymer segment inside the capsid is approximately half of the inner circumference of the capsid πR_0. For a clearly longer polymer segment the forces due to multiple contacts with the capsid wall point in several directions. This results in smaller measured resultant force.

E. Cumulative waiting times: Crossover to scaling

We define the cumulative waiting time $t(s)$ as the time it takes for the bead of index s to eject the capsid for the last time. In spite of the apparent scaling of τ with N_0, t does not scale with s for fully flexible polymers, as we have shown previously [15,16]. For verification of the pore models, Fig. 6(a) shows $t(s)$ obtained using the two different pores for different κ is
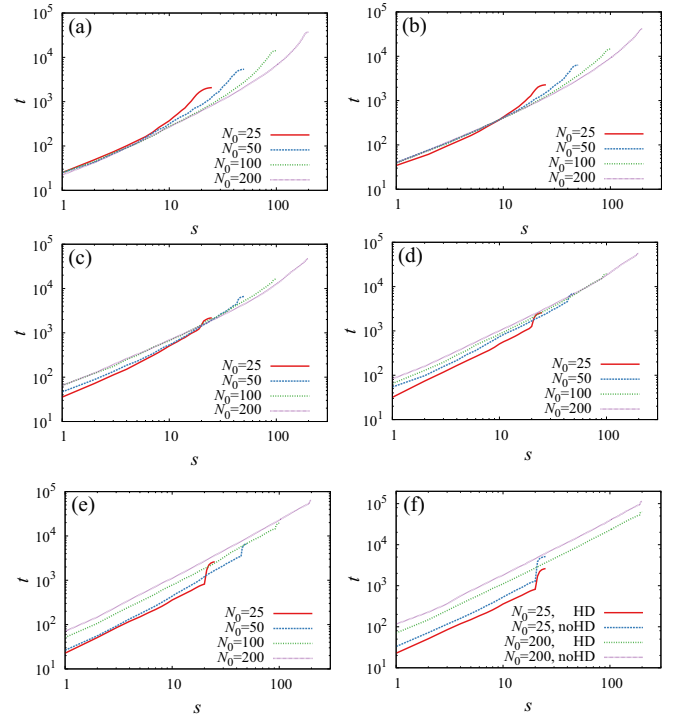

FIG. 7. Cumulative waiting times t vs s in logarithmic scale, with torus pore. (a–e) Hydrodynamics included, $\kappa = 0, 2.5, 5, 10, 20$. (f) With and without hydrodynamics, $\kappa = 20$.

shown for polymers of length $N_0 = 200$. The forms of $t(s)$ using the two pores are seen to be quite similar.

It is seen in Fig. 6(b) that, similarly to the fully flexible polymers, t does not scale with s for moderate and medium κ. However, for sufficiently rigid polymers scaling emerges. For $\kappa = 20$ perfect scaling $t \sim s^{1.33}$ is obtained for all N_0. Only at the end of the ejection there is the final diffusion of the polymers out of the capsid, during which $t(s)$ differs from the previous scaling relation. It is also evident from Fig. 6(a) that $t(s)$ increase with κ.

Figure 7 shows cumulative waiting times for each studied polymer length such that κ grows from Fig. 7(a) to Fig. 7(e) from $\kappa = 0$ to 20. When $\kappa = 20$ for the main part of the ejection where the monomer density inside the capsid is sufficiently high that the polymer is being pushed out of the capsid, the cumulative waiting times scale like $t \sim s^{1.33}$, whether hydrodynamics is included or not. Regarding the apparent scaling of the total ejection time $\tau \sim N_0^\beta$, the increase of β with κ for $\kappa \leqslant 10$ no longer holds for $\kappa = 20$, since transition to a different dynamical regime has taken place (see Table II).

Inclusion of hydrodynamics was seen to reduce β for all but the polymers of largest rigidity $\kappa = 20$ (see Table II). This effect comes from the final diffusive part of the ejection. For $\kappa = 20$ the diffusion at the final stage takes clearly longer for short polymers in the absence of hydrodynamics [see Fig. 7(f)]. The friction, which increases with κ, slows down the final diffusion of the polymer from the capsid. Hydrodynamic interactions reduce the friction of the diffusing rigid polymer tail. As seen in Fig. 7(f), for $\kappa = 20$ the contribution of the final diffusion on the total ejection time is largest for the shortest
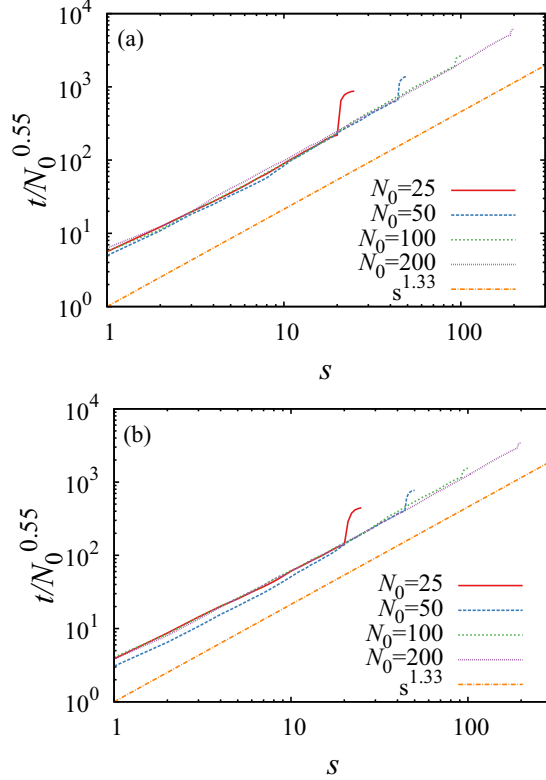
FIG. 8. Scaled cumulative waiting times $t(s)/N_0^{0.55}$ for $N_0 =$ 25, 50, 100, and 200 with $\kappa = 20$. (a) No hydrodynamics. (b) Hydrodynamics included. The separate dashed lines shows the scaling $\sim s^{1/3}$.

polymers, which reduces β. Since the friction of the diffusing tail is larger in the absence of hydrodynamics, β is larger when hydrodynamics is included.

For $\kappa \leqslant 10$ the inclusion of hydrodynamics, which reduces friction outside the pore, leads to enhanced relative friction due to the pore. Hence, the smaller β when including hydrodynamics and when using the cylinder pore comes from the same origin. This is similar to translocation where increasing the pore friction trivially takes the scaling toward linear [42].

As κ increases, there is a transition from exponential increase of t with s [15,16] to a regime where perfect scaling of $t \sim s^{1.33}$ emerges for the main part of the ejection. This transition has the characteristics of a dynamical phase transition, where κ acts as a control parameter. The scaling exponent equals $1 + \nu$, where $\nu = 1/3$ would be expected for a polymer driven through a pore from a spherical conformation in a way that relaxation does not appreciably change the conformation and the conformation is homogenous.

Alternatively, the crossover between the two dynamical regimes could be obtained by keeping ρ_0 and κ constant and varying the capsid radius R_0. Then R_0 would be the control parameter. Based on the above findings there would be a critical value for R_0 above which t increases with s exponentially and below which the scaling $t \sim s^{1.33}$ is obtained. If the scaling could be determined using moderate κ, polymers of reasonable lengths would suffice for determining R_0 where

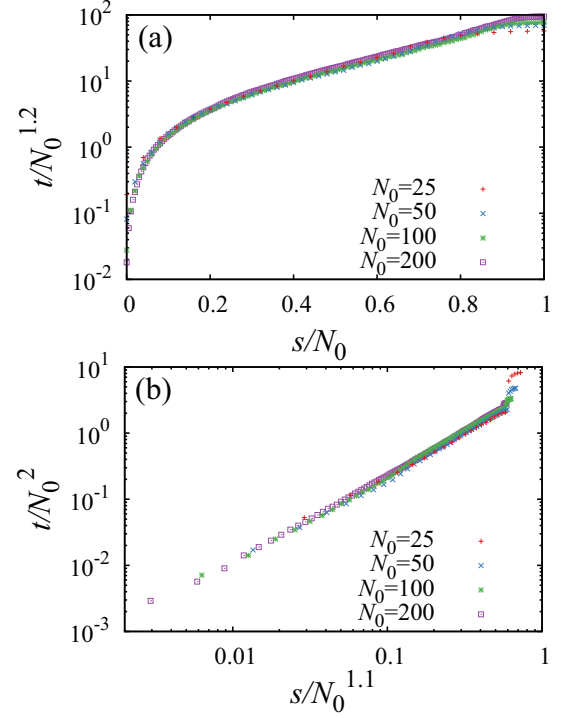FIG. 9. Data collapse for (a) $\kappa = 0$ and (b) $\kappa = 20$.

transition occurs. This alternative way of posing the capsid ejection problem is beyond the scope of the present paper.

Since simulated ejections for different N_0 start from a constant monomer density, Eq. (7), the capsid radius scales as $R_0 \sim N_0^{1/3}$. A semirigid polymer densely packaged inside a capsid is in a conformation where intertwined lobes fill the spherical volume. The angles and directions of these lobes vary randomly. Although for large κ ejection is slowed down, the conformations do not appreciably change due to relaxation for $\kappa = 20$, since the persistence length is clearly greater than the capsid diameter. (From Table I, $\lambda_p \approx 21.9$ for $\kappa = 20$ and $N_0 = 200$. The diameter of the capsid used for this polymer is roughly 8.) Hence, the measured $t(s)$, which is an average over ejections, reflects the initial random conformations. The spherical scaling of the ejection of the randomly oriented rigid segments would seem to result from the spherical confinement.

F. Scaling functions

For $\kappa = 20$, the force f multiplied by $N_0^{0.4}$ plotted as a function of s/N_0 approximately collapses in a large range [see Fig. 5(b)]. Therefore, it is reasonable to expect that such a data collapse exists also for the cumulative waiting time t. This, indeed, is the case. Figure 8 shows the cumulative waiting times $t(s)$ for different N_0 scaled by $1/N_0^{0.55}$. The parts of $t(s)/N_0^{0.55}$ scaling as $\sim s^{1.33}$ are seen to fall on top of each other. The scaling of force $f \sim 1/N_0^{0.4}$ for each s/N_0 naturally shows as scaling in the cumulative waiting time magnitudes. The cumulative waiting time for sufficiently rigid polymers in the regime where the polymer is driven by the pressure inside the capsid can thus be written as

$$t(s) \propto N_0^{0.55} s^{1.33} \qquad (10)$$

both in the absence and presence of hydrodynamics. The prefactor $N_0^{0.55}$ indicates that it may be possible to select capsid volumes for different N_0 such that the scaling parts of $t(s)$ have the same magnitude. The initial condition, which for fully flexible polymers was judiciously chosen as starting from constant monomer density, needs to be modified to take into account the relation of the persistence length to the capsid radius and the polymer length, among other things.

Finally, we note that for each κ a single scaling function can be found to describe the measured cumulative waiting times of polymers of different N_0. Figure 9 shows the data collapse for the minimum and maximum rigidities used in our paper. The cumulative waiting times can be expressed by the corresponding scaling functions as $t(s,N_0) = N_0^{1.2}\Gamma(s/N_0)$ for $\kappa = 0$ and $t(s,N_0) = N_0^2\Psi(s/N_0^{1.1})$ for $\kappa = 20$. It should be borne in mind that precise exponent values can be obtained only when finite-size effects, such as the density correction, are taken properly into account. A scaling function that would describe t in a small range of κ around $\kappa = \kappa_c$, where κ_c is the value at which the transition to $t \sim s^{1.33}$ occurs, could serve as a starting point for a renormalization group approach for a universal description of the dynamical transition as a function of polymer rigidity.

IV. CONCLUSION

We have studied the ejection of semiflexible polymers from a spherical capsid and under initial strong confinement. The ejection simulations were performed by stochastic rotation dynamics, which is a molecular dynamics based method where inclusion of hydrodynamic modes is possible. The capsid was implemented via simple boundary conditions and the effect of geometrical pore friction was minimized using a torus pore with perfectly round edges. This pore implementation was validated by comparison to the previously used cylinder pore. The initial conformations were generated by capsid injection using Langevin dynamics.

We found that the rate at which polymers are packaged inside the capsid affects the ejection time. The conformations that were allowed less time for equilibration during packaging ejected faster. This characteristics is likely related to the deeper local energy minima of the conformations that were allowed to relax for a longer time. The time allowed for equilibration was chosen such that increasing this time further did not change the ejection time appreciably. By measurements of the radius of gyration for the polymer segment outside the capsid during ejection we found that all contribution to the change in the dynamics with the polymer length N_0 comes from inside the capsid.

Unlike in the case of fully flexible polymers, we found that for semiflexible polymers with $\kappa = 20$ the force f measured at the pore has no clear relation to the measured monomer ejection times. f showed clear dependence on the polymer length such that the force magnitudes as a function of s/N_0 scaled like $f \sim N_0^{-0.4}$.

There are basically two regimes in ejection dynamics. For the main part monomer density in the capsid is sufficiently high that the polymer is being driven out through the pore. In the second regime at the end of ejection the remaining segment diffuses out of the capsid. For low κ the regimes are overlapping. This overlap diminishes as κ is increased and scaling of the cumulative waiting time t with s emerges. For $\kappa = 20$ the regimes are clearly separate and perfect scaling of $t(s) \sim s^{1.33}$ is obtained for the driven regime both in the absence and presence of hydrodynamic interactions. The scaling exponent is precisely $1 + \nu$, where $\nu = 1/3$ is the scaling for the radius R of spherically confined polymer conformations $R \sim N_0^\nu$. We gave some arguments for obtaining $t(s) \sim s^{1+\nu}$ when averaged over many individual ejections of sufficiently rigid polymers.

Hydrodynamics was found to speed up the ejection at all stages. The speedup was strongest in the diffusion regime at the end of the process, where hydrodynamic interactions lower the friction caused by the rigid tail inside the capsid. We found a perfect collapse for the scaled cumulative waiting times in the driven regime $t(s)/N_0^{0.55}$. Consequently, the cumulative waiting time for the driven part can be expressed as $t(s) \propto N_0^{0.55}s^{1.33}$.

A very good data collapse for the cumulative waiting times for different N_0 was found in the whole rigidity range investigated here. The measured cumulative waiting times can be expressed compactly with the scaling functions as $t(s,N_0) = N_0^{1.2}\Gamma(s/N_0)$ for $\kappa = 0$ and $t(s,N_0) = N_0^2\Psi(s/N_0^{1.1})$ for $\kappa = 20$. For the semirigid polymers the scaling function applies for the driven regime. Similar scaling functions can be found for all intermittent values of κ. These scaling functions suggest that there may exist a valid scaling hypothesis for the free energy of the confined polymers that would lead to correct ejection dynamics.

[1] P. Grayson, L. Han, T. Winther, and R. Phillips, Real-time observations of single bacteriophage λ DNA ejections in vitro, Proc. Natl. Acad. Sci. USA **104**, 14652 (2007).

[2] D. Panja and I. J. Molineux, Dynamics of bacteriophage genome ejection, Phys. Biol. **7**, 045006 (2010).

[3] I. J. Molineux and D. Panja, Popping the cork: Mechanisms of phage genome ejection, Nat. Rev. Microbiol. **11**, 194 (2013).

[4] J. Glasgow and D. Tullman-Ercek, Production and applications of engineered viral capsids, Appl. Microbiol. Biotechnol. **98**, 5847 (2014).

[5] Y. Erlich and D. Zielinski, DNA fountain enables a robust and efficient storage architecture, Science **355**, 950 (2017).

[6] M. Muthukumar, Translocation of a Confined Polymer Through a Hole, Phys. Rev. Lett. **86**, 3188 (2001).

[7] A. Cacciuto and E. Luijten, Confinement-Driven Translocation of a Flexible Polymer, Phys. Rev. Lett. **96**, 238104 (2006).

[8] A. Y. Grosberg and A. R. Khokhlov, *Statistical Physics of Macromolecules* (American Institute of Physics, New York, 1994).

[9] T. Sakaue and E. Raphaël, Polymer chains in confined spaces and flow-injection problems: Some remarks, Macromolecules **39**, 2621 (2006).

[10] T. Sakaue and N. Yoshinaga, Dynamics of Polymer Decompression: Expansion, Unfolding, and Ejection, Phys. Rev. Lett. **102**, 148302 (2009).

[11] I. Ali, D. Marenduzzo, and J. M. Yeomans, Polymer Packaging and Ejection in Viral Capsids: Shape Matters, Phys. Rev. Lett. **96**, 208102 (2006).

[12] I. Ali, D. Marenduzzo, and J. Yeomans, Ejection dynamics of polymeric chains from viral capsids: Effect of solvent quality, Biophysical Journal **94**, 4159 (2008).

[13] A. Al Lawati, I. Ali, and M. Al Barwani, Effect of temperature and capsid tail on the packing and ejection of viral DNA, PLOS ONE **8**, e52958 (2013).

[14] R. P. Linna, J. E. Moisio, M. Suhonen, and K. Kaski, Dynamics of polymer ejection from capsid, Phys. Rev. E **89**, 052702 (2014).

[15] J. Piili and R. P. Linna, Polymer ejection from strong spherical confinement, Phys. Rev. E **92**, 062715 (2015).

[16] J. Piili, M. Suhonen, and R. P. Linna, Uniform description of polymer ejection dynamics from capsid with and without hydrodynamics, Phys. Rev. E **95**, 052418 (2017).

[17] J. Mahalik, B. Hildebrandt, and M. Muthukumar, Langevin dynamics simulation of DNA ejection from a phage, Journal of Biological Physics **39**, 229 (2013).

[18] A. S. Petrov, S. S. Douglas, and S. Harvey, Effects of pulling forces, osmotic pressure, condensing agents and viscosity thermodynamics and kinetics of DNA ejection from bacteriophages to bacterial cells: A computational study, J. Phys.: Condens. Matter **25**, 115101 (2013).

[19] B. Alberts, A. Johnson, J. Lewis, D. Morgan, M. Raff, K. Roberts, and P. Walter, *Molecular Biology of the Cell*, 6th ed. (Garland Science, New York, 2014), pp. 1266, 1273, 1274, 1280.

[20] D. Marenduzzo, C. Micheletti, E. Orlandini, and D. W. Sumners, Topological friction strongly affects viral DNA ejection, Proc. Natl. Acad. Sci. USA **110**, 20081 (2013).

[21] D. Marenduzzo, E. Orlandini, A. Stasiak, D. W. Sumners, L. Tubiana, and C. Micheletti, DNA–DNA interactions in bacteriophage capsids are responsible for the observed DNA knotting, Proc. Natl. Acad. Sci. USA **106**, 22269 (2009).

[22] A. Matsuyama and M. Yano, Ejection dynamics of a semiflexible DNA polymer from a capsid, J. Phys. Soc. Jpn. **81**, 034802 (2012).

[23] R. P. Linna and K. Kaski, Analysis of DNA Elasticity, Phys. Rev. Lett. **100**, 168104 (2008).

[24] G. S. Manning, The persistence length of DNA is reached from the persistence length of its null isomer through an internal electrostatic stretching force, Biophys. J. **91**, 3607 (2006).

[25] D. Van Valen, D. Wu, Y.-J. Chen, H. Tuson, Wiggins, and R. Phillips, A single-molecule hershey-chase experiment, Curr. Biol. **22**, 1339 (2012).

[26] A. Malevanets and R. Kapral, Mesoscopic model for solvent dynamics, J. Chem. Phys. **110**, 8605 (1999).

[27] A. Malevanets and R. Kapral, Mesoscopic multi-particle collision model for fluid flow and molecular dynamics, in *Novel Methods in Soft Matter Simulations*, edited by M. Karttunen, A. Lukkarinen, and I. Vattulainen, Lecture Notes in Physics Vol. 640 (Springer-Verlag, Berlin, Heidelberg, 2004).

[28] G. Gompper, T. Ihle, D. Kroll, and R. Winkler, Multi-particle collision dynamics: A particle-based mesoscale simulation approach to the hydrodynamics of complex fluids, in *Advanced Computer Simulation Approaches for Soft Matter Sciences*, edited by C. Holm and K. Kremer, Advances in Polymer Science Vol. 221 (Springer, Berlin, 2009).

[29] T. Ihle and D. M. Kroll, Stochastic rotation dynamics: A galilean-invariant mesoscopic model for fluid flow, Phys. Rev. E **63**, 020201 (2001).

[30] D. Frenkel and B. Smit, *Understanding Molecular Simulation: From Algorithms to Applications* (Academic, New York, 2001).

[31] W. C. Swope, H. C. Andersen, H. Berens, and K. R. Wilson, A computer simulation method for the calculation of equilibrium constants for the formation of physical clusters of molecules: Application to small water clusters, J. Chem. Phys. **76**, 637 (1982).

[32] D. L. Ermak and H. Buckholz, Numerical integration of the Langevin equation: Monte Carlo simulation, J. Comput. Phys. **35**, 169 (1980).

[33] G. Wyvill and L. T. Kunii, A functional model for constructive solid geometry, The Visual Computer **1**, 3 (1985).

[34] A. Lamura, G. Gompper, T. Ihle, and D. M. Kroll, Multi-particle collision dynamics: Flow around a circular and a square cylinder, Europhys. Lett. **56**, 319 (2001).

[35] M. E. Cerritelli, N. Cheng, A. H. Rosenberg, C. E. McPherson, F. P. Booy, and A. C. Steven, Encapsidated conformation of bacteriophage T7 DNA, Cell **91**, 271 (1997).

[36] C. Forrey and M. Muthukumar, Langevin dynamics simulations of genome packing in bacteriophage, Biophys. J. **91**, 25 (2006).

[37] D. C. Rapaport, Packaging stiff polymers in small containers: A molecular dynamics study, Phys. Rev. E **94**, 030401 (2016).

[38] N. Stoop, J. Najafi, F. K. Wittel, M. Habibi, and H. J. Herrmann, Packing of Elastic Wires in Spherical Cavities, Phys. Rev. Lett. **106**, 214102 (2011).

[39] R. Matthews, A. A. Louis, and J. M. Yeomans, Knot-Controlled Ejection of a Polymer from a Virus Capsid, Phys. Rev. Lett. **102**, 088101 (2009).

[40] C. R. Locker, S. D. Fuller, and S. C. Harvey, DNA organization and thermodynamics during viral packing, Biophys. J. **93**, 2861 (2007).

[41] H.-P. Hsu and K. Binder, Stretching semiflexible polymer chains: evidence for the importance of excluded volume effects from monte carlo simulation, J. Chem. Phys. **136**, 024901 (2012).

[42] V. V. Lehtola, R. P. Linna, and K. Kaski, Dynamics of forced biopolymer translocation, Europhys. Lett. **85**, 58006 (2009).